Results in Physics 16 (2020) 102818

Contents lists available at ScienceDirect

Results in Physics

journal homepage: www.elsevier.com/locate/rinp

MHD natural convection of Sodium Alginate Casson nanofluid over a solid sphere

Firas A. Alwawi[a,b,*], Hamzeh T. Alkasasbeh[c], A.M. Rashad[d], Ruwaidiah Idris[a]

[a] School of Informatics and Applied Mathematics, Universiti Malaysia Terengganu, 21030 Kuala Terengganu, Terengganu, Malaysia
[b] Department of Mathematics, College of Sciences and Humanities in Al-Kharj, Prince Sattam bin Abdulaziz University, Al-Kharj 11942, Saudi Arabia
[c] Department of Mathematics, Faculty of Science, Ajloun National University, P.O. Box 43, Ajloun 26810, Jordan
[d] Department of Mathematics, Aswan University, Faculty of Science, Aswan 81528, Egypt

ARTICLE INFO

Keywords:
Casson nanofluid
MHD
Natural convection
Sodium alginate
Solid sphere

ABSTRACT

MHD free convection flow of Sodium Alginate nanofluid on a solid sphere with prescribed wall temperature is investigated. Tiwari and Das's nanofluid model is applied to analyze the influence of nanoparticles and magnetic field on a natural convective flow. Titanium dioxide (TiO_2), Silver (Ag), and Graphite oxide (GO) Sodium Alginate-based nanofluid has been considered. The Keller-box method is employed to solve the transformed system of partial differential equations. The impact of Casson fluid parameter, magnetic parameter, nanoparticles volume fraction on local skin friction coefficient, local Nusselt number, temperature, and velocity are plotted and analyzed. Our graphical results revealed that the (GO)- Sodium Alginate based Casson nanofluid has the highest local skin friction, local Nusselt number and velocity profiles as compared to the other nanoparticles Sodium Alginate based Casson nanofluid.

Introduction

Sodium alginate is a natural Casson fluid extracted from brown algae; it is highly viscous, safe and has a water solubility. These properties make sodium alginate widely used in variety applications, such as food manufacturing, pharmaceuticals, textiles and cosmetics. Sodium alginate was first discovered by the British pharmacist Edward C. Stanford in 1881 [1,2]. Later on, numerous articles have been done on the field of Sodium alginate flow. Hatami and Ganji [3] analyzed heat transfer and flow for Sodium alginate nanofluid in the porous medium between two coaxial cylinders. Hatami and Ganji [4] examined the free convection flow of Sodium alginate nanofluid between two vertical flat plates. Akinshilo et al. [5] studied the flow of copper Sodium Alginate-based Casson nanofluid conveying nanoparticles within two vertical parallel plates. Sharma et al. [6] applied the Homotopy analysis method to examine the unsteady MHD mixed convection of Sodium alginate with a stretching/shrinking wedge. Ahmed and Khan [7] analyzed the mixed convection flow of Sodium alginate nanofluids over an infinite vertical plate. Tlili et al. [8] studied the influence of multiple Slips on steady convection of Sodium Alginate nanofluid on a stretching porous cylinder in the existence of thermal radition, magnetic field and chemical reaction.

Due to poor thermal properties of the ordinary base fluids, for instance, water, ethylene glycol, and engine oil, a new subclass of fluids known as nanofluids have been developed, which consists of nanoparticles suspended in a host fluid. The main goal behind the addition of nanoparticles is to enhance the thermal properties for conventional host fluids at the lowest concentrations of these suspensions. The nanoparticles are usually made of Al_2O_3, SiC, AlN, Cu, and TiO_2 graphite oxide. The concept of nanofluids was first reported by Choi and Estman [9], where they introduced the idea of nanoparticles suspended in a host fluid. Recently, two mathematical models are utilized extensively to anlayaze the behavior of nanofluids specifically, Buongiorno's model [10] and Tiwari-Das's model [11].

Buongiorno's model is a two-phase model focused on Brownian motion and thermophoresis effects while Tiwari-Das's model is a single-phase model concerned with studying volume fraction of nanoparticles, [12–19] investigated behavior of nanofluids by utlizing Tiwari-Das's model, and [20–24] used Buongiorno's model. Further reading, see the following comprehensive references [25–28]. MHD Natural convection over a sphere has been gotten much consideration by many researchers due to it's applications in several industrial and mechanical, where an enormous articles have been published in the same field. Kumari et al. [29] utilized the shooting method to investigate the problem of MHD flow of an electrically conducting fluid in the stagnation region of a sphere. Nazar and Amin [30] examined the free convection flow on

* Corresponding author.
E-mail address: f.alwawi@psau.edu.sa (F.A. Alwawi).

https://doi.org/10.1016/j.rinp.2019.102818
Received 25 January 2019; Received in revised form 17 November 2019; Accepted 18 November 2019
Available online 23 November 2019

Nomenclature

k_{nf}	Thermal conductivity of nanofluid
k_s	Thermal conductivity of nanoparticles
k_f	Thermal conductivity of base fluid
T	Temperature of the fluid
T_w	Wall temperature
T_∞	Ambient\;temperature
v_f	Kinematic viscosity of base fluid
v	x - component of velocity
v	y - component of velocity
M	Magnetic parameter
Pr	Prandtl number
Gr	Grashof number
C_f	Local skin friction coefficient
Nu	Local Nusselt number
a	Radius of\;solid sphere
$r(x)$	Radial distance
g	Gravity vector
p_y	Yield stress of the fluid
ψ	Streem function
τ_w	Wall shear stress
q_w	Wall heat flux
σ_f	Electrical conductivity of\;base fluid
σ_{nf}	Electrical conductivity of\;nanofluid
$(\rho c_p)_{nf}$	Heat capacity of nanofluid
$(\rho c_p)_s$	Heat capacity of nanoparticles
$(\rho c_p)_s$	Heat capacity of base fluid
β	Casson parameter
χ	Volume fraction of nanoparticles
β_f	Thermal expansion of base fluid
β_s	Thermal expansion of nanoparticles
ρ_f	Density of base fluid
ρ_s	Density of nanoparticles
ρ_{nf}	Density of nanofluid
μ_{nf}	Dynamic viscosity of nanofluid
μ_f	Dynamic viscosity of the base fluid
μ_β	Plastic dynamic viscosity\;of the base fluid
θ	Temperature\;of\;\;nanofluid
π	Product of the component of deformation rate
B_0	Magnetic field strength
e_{ij}	(i, j) − th component of the deformation rate
π_c	Critical value of the product π
α_f	Thermal diffusivity of base fluid
α_{nf}	Thermal diffusivity of nanofluid

isothermal sphere in a micropolar fluid. Chamkha and Al-Mudhaf [31] studied the impact of magnetic field and thermal radiation on natural convection from a permeable sphere. Alkasasbeh [32] investigated MHD free convection flow of Casson micropolar fluid on a solid sphere. Also, [33–36] all of them examined the influence of heat generation and magnetic field on free convection over a sphere.

According to the previous studies, MHD natural convection flow of Casson nanofluid on a solid sphere with prescribed wall temperature is not investigated. Therefore, the present article examines the free convection flow of Casson nanofluid in the prsence of magnetic field. The relevant partial differential equations are first converted into non-dimensional equations by using appropriate transformation and then computed by utilizing the Keller box method.

The important observations of our study are listed in the conclusions.

Mathematical formulation

Consider the steady laminar 2-D incompressible magneto-hydrodynamic free convection flow of Silver (Ag), Titanium dioxide (TiO_2) and Graphite oxide (GO) Sodium Alginate – based Casson nanofluid over a solid sphere of the radius $a$and constant wall temperature T_w as shown in Fig. 1. where $g$is the gravity vector, x^*- coordinate is measured along the surface of the solid sphere at the lower stagnation point $(x^* \approx 0)$, y^*- coordinate is measured the distance normal to the surface of the sphere and $r^*(x^*)$ is the radial distance from the symmetrical axis to the surface of the solid sphere. A uniform magnetic field B_0 is utilized in the direction perpendicular to the surface.

In the beginning, the temperature of the solid sphere and the Casson nanofluid are kept equal. Instantly they are increased to a temperature $T_w > T_\infty$, the ambient temperature of the fluid which stays fixed. The Casson fluid flow is given by Hatami and Ganji [3,4]

$$\tau_{ij} = \begin{cases} 2(\mu_B + p_y\sqrt{2\pi})e_{ij} & \pi > \pi_c, \\ 2(\mu_B + p_y\sqrt{2\pi_c})e_{ij} & \pi < \pi_c, \end{cases} \tag{1}$$

here $\pi = e_{ij}e_{ij}$, e_{ij} is the (i, j)-th component of the deformation rate, μ_β is the plastic dynamic viscosity of the non-Newtonian fluid, p_y is the yield stress of the fluid and π_c is a critical value of this product based on the non-Newtonian model. Introducing the boundary layer approximations of a Casson nanofluid, the continuity, momentum and energy

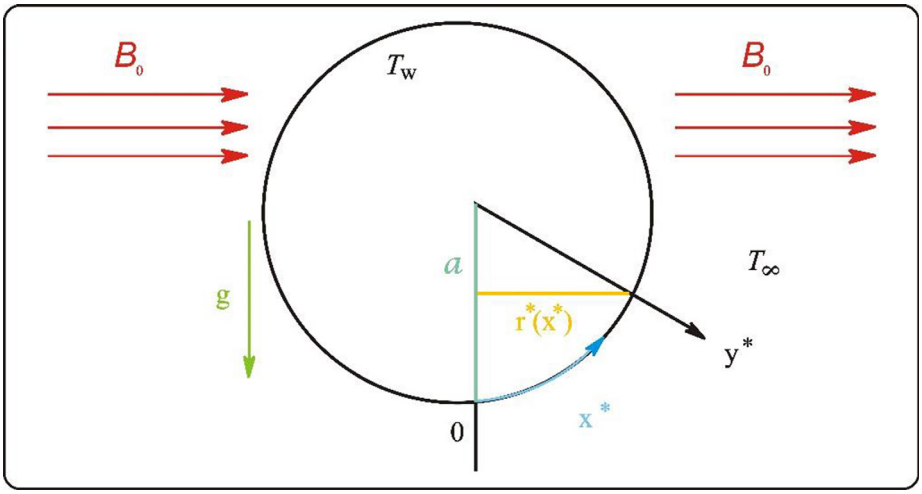

Fig. 1. Physical model and coordinate system.

Table 1
Thermo-physical properties of Ag, TiO_2, GO and SA as a based Casson fluid [37,47–49].

Thermo-Physical property	SA	Ag	TiO_2	GO
$\rho(kg/m^3)$	989	10,500	4230	1800
$C_p(J/kgK)$	4175	235	650	717
$K(w/mK)$	0.6376	429	8.9528	5000
$\beta \times 10^{-5}(K^{-1})$	99	1.89	0.9	28.4
$\sigma(s/m)$	2.6×10^{-4}	6.3×10^{7}	2.6×10^{6}	1.1×10^{-5}
Pr	6.5	–	–	–

Table 2
A numerical Comparison of present results for local Nusselt number $Gr^{-1/4}Nu$, with pervious published results, at Pr = 0.7, $\chi = 0$, $M = 0$, and $\beta \to \infty$.

x	Huang and Chen [44]	Molla et al. [45]	Cheng [46]	Present
0°	0.4574	0.4576	0.4576	0.4576
10°	0.4563	0.4564	0.4565	0.4565
20°	0.4532	0.4532	0.4534	0.4534
30°	0.4480	0.4479	0.4481	0.4480
40°	0.4407	0.4404	0.4407	0.4406
50°	0.4312	0.4307	0.4310	0.4310
60°	0.4194	0.4188	0.4191	0.4194
70°	0.4053	0.4045	0.4049	0.4053
80°	0.3886	0.3877	0.3881	0.3886
90°	0.3684	0.3683	0.3686	0.3693
100°	–	–	–	0.3470
110°	–	–	–	0.3216
120°	–	–	–	0.2927

equations, respectively are expressed as:

$$\frac{\partial}{\partial x^*}(r^* u^*) + \frac{\partial}{\partial y^*}(r^* v^*) = 0, \tag{2}$$

$$u^*\frac{\partial u^*}{\partial x^*} + v^*\frac{\partial u^*}{\partial y^*} = \frac{\mu_{nf}}{\rho_{nf}}\left(1 + \frac{1}{\beta}\right)\frac{\partial^2 u^*}{\partial y^{*2}} + \left(\frac{\chi\rho_s\beta_s + (1-\chi)\rho_f\beta_f}{\rho_{nf}}\right)g(T - T_\infty)\sin\left(\frac{x^*}{a}\right) - \frac{\sigma_{nf}B_0^2}{\rho_{nf}}u^*, \tag{3}$$

$$u^*\frac{\partial T}{\partial x^*} + v^*\frac{\partial T}{\partial y^*} = \alpha_{nf}\frac{\partial^2 T}{\partial y^{*2}}, \tag{4}$$

Corresponding to the boundary conditions which are given by Akinshilo et al. [5]

$$u^* = v^* = 0,\ T = T_w,\ as y^* = 0,$$

$$u^* \to 0,\ T \to T_\infty,\ as\ y^* \to \infty. \tag{5}$$

where $\beta = \mu_\beta\sqrt{2\pi_c}/p_y$ is the Casson fluid parameter, $B_0^2$is the Magnetic field strength and

$r^*(x^*)$is the radial distance from the symmetrical axis to the surface of the solid sphere and

$$r^*(x^*) = a\sin\left(\frac{x^*}{a}\right) \tag{6}$$

Now, we will introduce the following non-dimensional variables (are defined by Trisaksri and Wongwises [27])

$$x = \frac{x^*}{a},\ y = Gr^{1/4}\left(\frac{y^*}{a}\right),\ r = \frac{r^*}{a},\ u = \left(\frac{a}{\nu_f}\right)Gr^{-1/2}u^*,\ v = \left(\frac{a}{\nu_f}\right)Gr^{-1/4}v^*,\ \theta = \frac{T - T_\infty}{T_w - T_\infty} \tag{7}$$

where $Gr = g\beta_f(T_w - T_\infty)\frac{a^3}{\nu_f^2}$ is the Grashof number. Substitute Eqs. (6) and (7) into Eqs. (2)–(5), to get the following nondimensional equations:

$$\frac{\partial}{\partial x}(ru) + \frac{\partial}{\partial y}(rv) = 0, \tag{8}$$

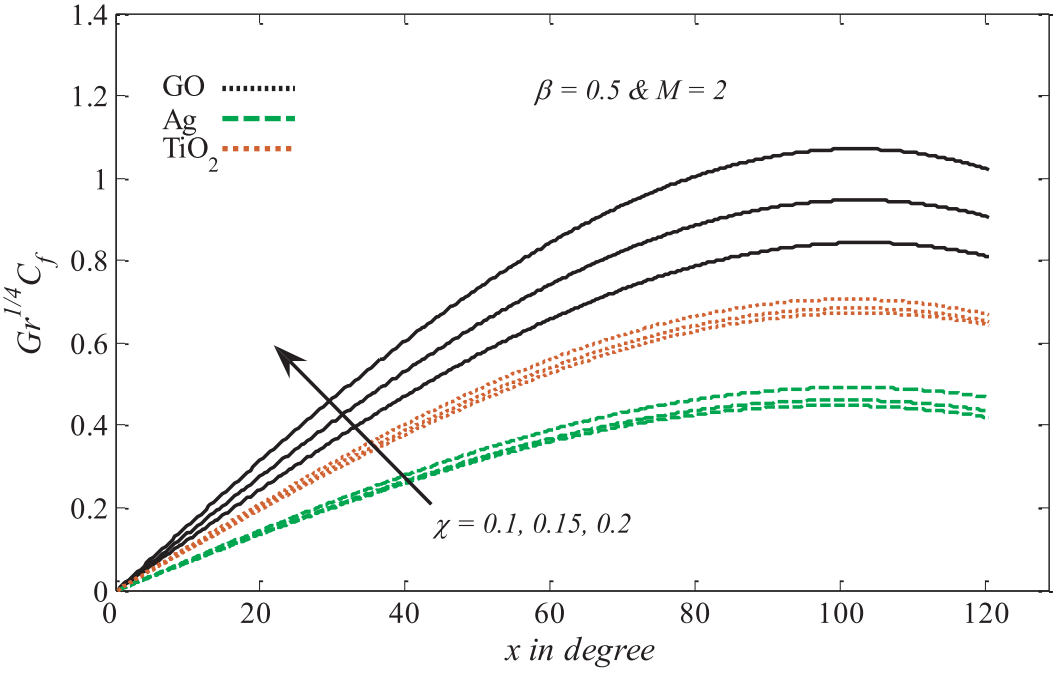

Fig. 2. χ vs $Gr^{1/4}C_f$

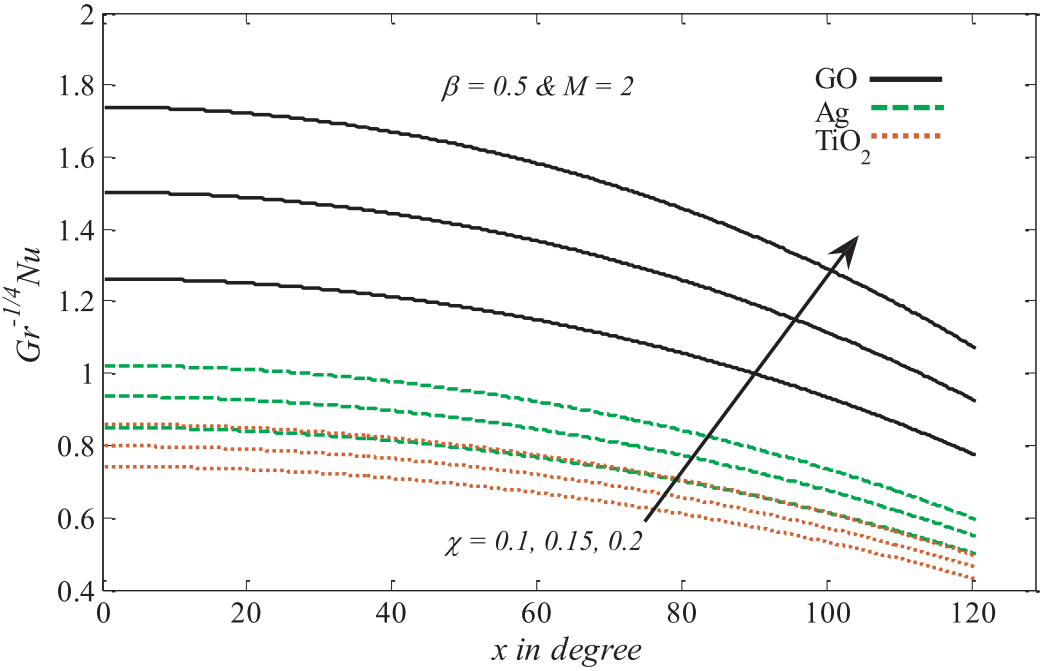

Fig. 3. χ vs $Gr^{-1/4}Nu$

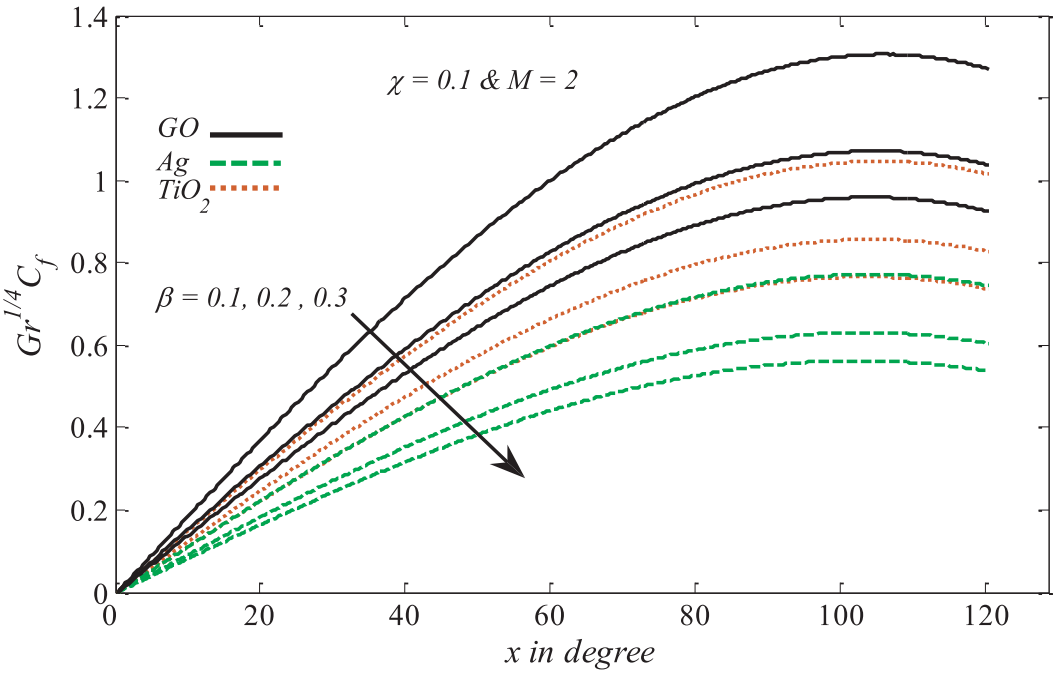

Fig. 4. β vs $Gr^{1/4}C_f$

$$u\frac{\partial u}{\partial x} + v\frac{\partial u}{\partial y} = \frac{\rho_f}{\rho_{nf}}\frac{1}{(1-\chi)^{2.5}}\left(1+\frac{1}{\beta}\right)\frac{\partial^2 u}{\partial y^2} + \left(\frac{\chi\rho_s\beta_s/\beta_f + (1-\chi)\rho_f}{\rho_{nf}}\right)\theta\sin x - \frac{\rho_f}{\rho_{nf}}\frac{\sigma_{nf}}{\sigma_f}Mu, \tag{9}$$

$$u\frac{\partial\theta}{\partial x} + v\frac{\partial\theta}{\partial y} = \frac{1}{\Pr}\left(\frac{k_{nf}/k_f}{(1-\chi)+\chi(\rho c_p)_s/(\rho c_p)_f}\right)\frac{\partial^2\theta}{\partial y^2}, \tag{10}$$

with boundary conditions

$$u = v = 0,\ \theta = 1,\ as\ y = 0,$$

$$u \to 0,\ u \to 0,\ \theta \to 0,\ as\ y \to \infty. \tag{11}$$

where $M = \left(\frac{\sigma_f B_0^2 a^2 Gr^{\frac{-1}{2}}}{\rho_f \nu_f}\right)$ is the magnetic parameter, $\Pr = \frac{\nu_f}{\alpha_f}$ is the Prandtl number,

Moreover, the quantities σ_{nf}, k_{nf}, μ_{nf}, $(\rho c_p)_{nf}$, ρ_{nf} and α_{nf} are introduced by [37–39] as:

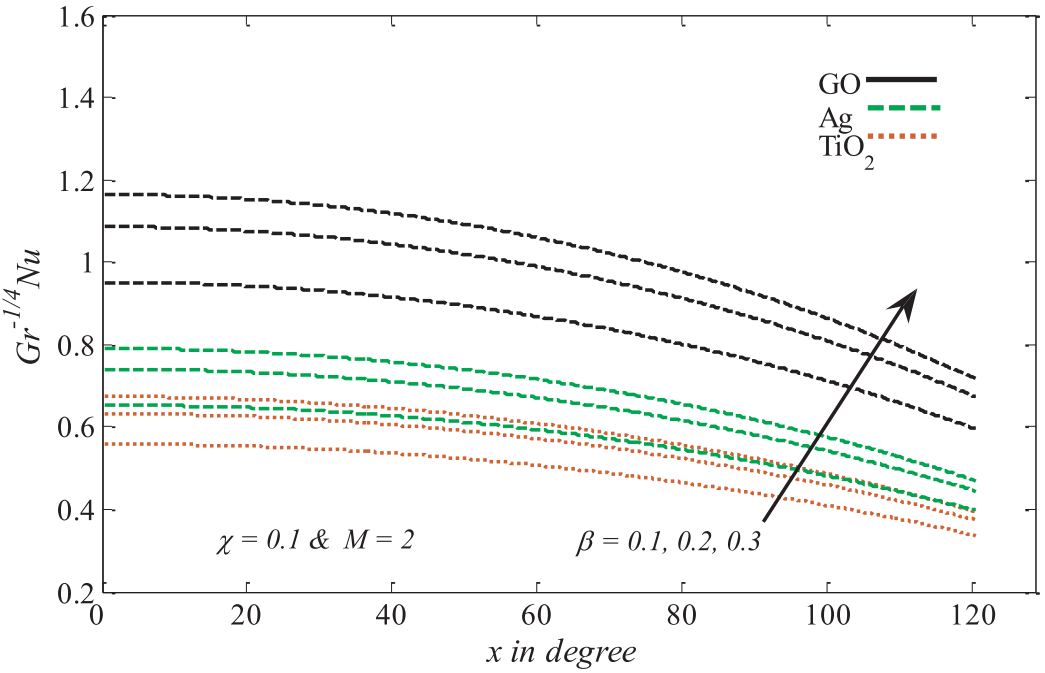

Fig. 5. β vs $Gr^{-1/4}Nu$

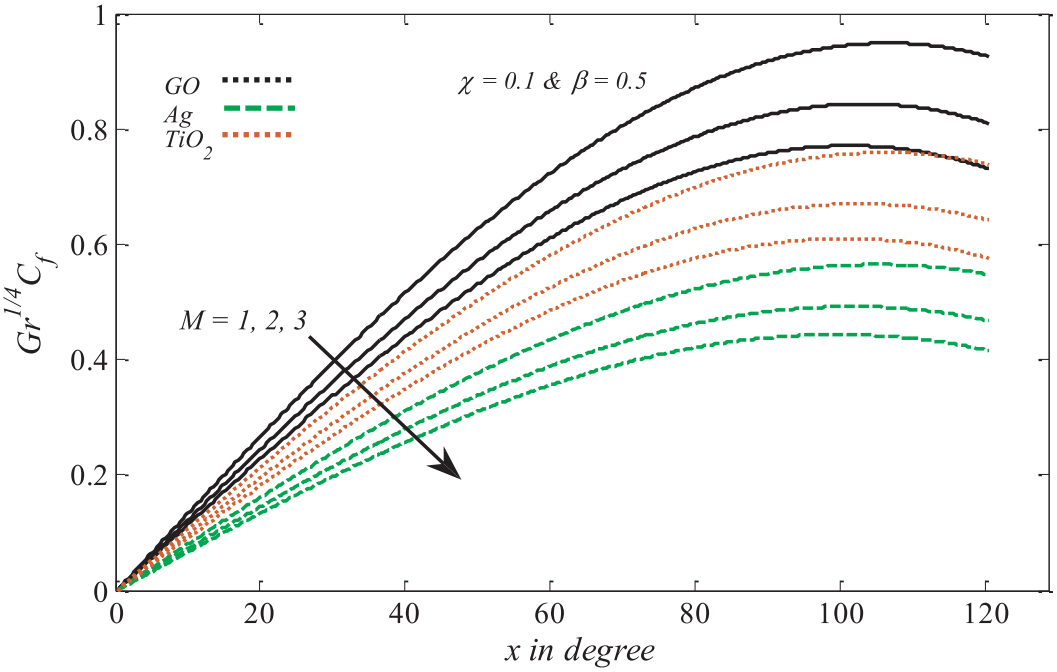

Fig. 6. M vs $Gr^{1/4}C_f$

$$\frac{\sigma_{nf}}{\sigma_f} = 1 + \frac{3(\sigma-1)\chi}{(\sigma+2)-(\sigma-1)\chi}, \quad \sigma = \frac{\sigma_s}{\sigma_f},$$
$$\frac{k_{nf}}{k_f} = \frac{(k_s+2k_f)-2\chi(k_f-k_s)}{(k_s+2k_f)+\chi(k_f-k_s)}, \quad \mu_{nf} = \frac{\mu_f}{(1-\chi)^{2.5}},$$

$$(\rho c_p)_{nf} = (1-\chi)(\rho c_p)_f + \chi(\rho c_p)_s, \quad \rho_{nf} = (1-\chi)\rho_f + \chi\rho_s,$$
$$\alpha_{nf} = \frac{k_{nf}}{(\rho c_p)_{nf}}, \tag{12}$$

To solve Eqs. (8)–(10), along with the boundary conditions (11), defined the following variables (Swalmeh et al. [40]):

$$\psi = xr(x)F(x,y), \quad \theta = \theta(x,y), \tag{13}$$

where ψ is the stream function expressed as :

$$u = \frac{1}{r}\frac{\partial\psi}{\partial y} \text{ and } v = -\frac{1}{r}\frac{\partial\psi}{\partial x}, \tag{14}$$

which satisfies Eq. (9). Thus, Eqs. (10) and (11) can be written as follows:

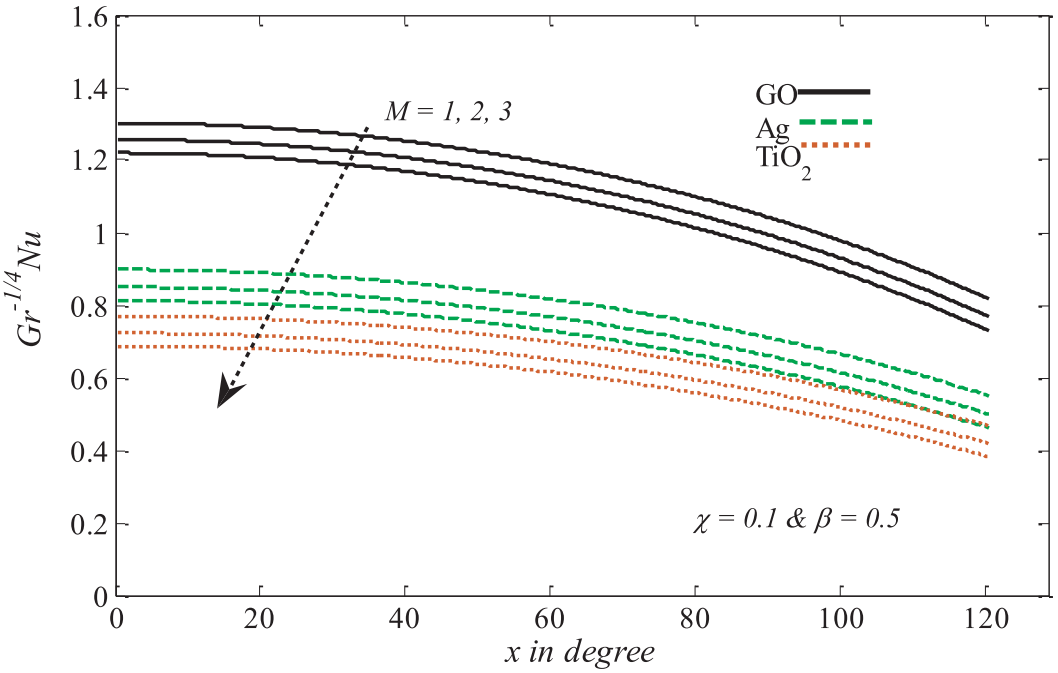

Fig. 7. M vs $Gr^{-1/4}Nu$

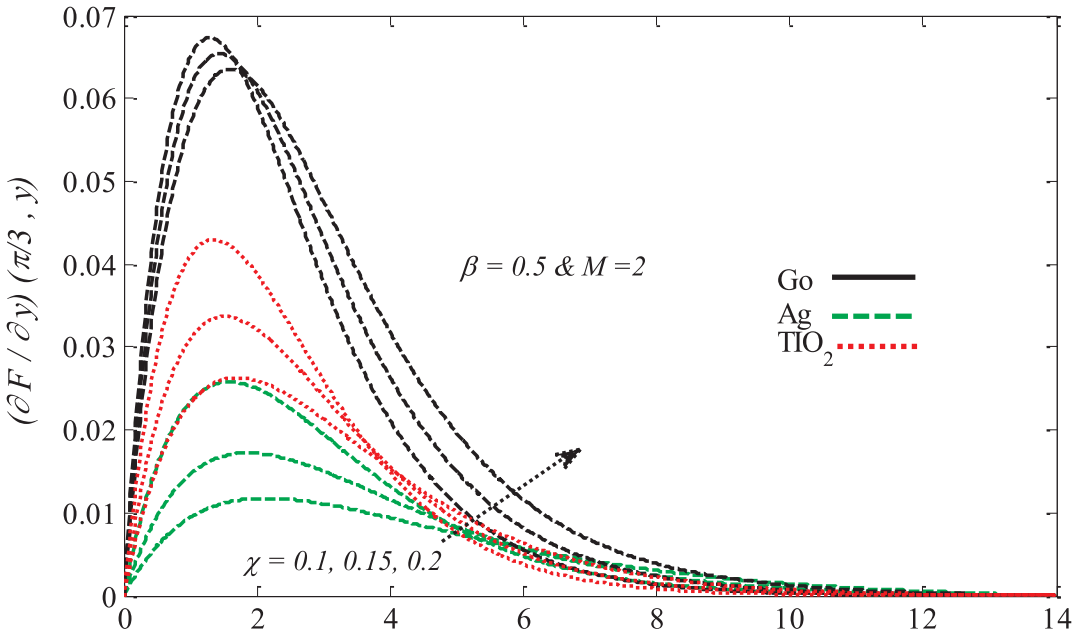

Fig. 8. χ vs $(\partial F/\partial y)(\pi/3\ ,\ y)$

$$\frac{\rho_f}{\rho_{nf}}\frac{1}{(1-\chi)^{2.5}}\left(1+\frac{1}{\beta}\right)\frac{\partial^3 F}{\partial y^3}+(1+x\cot x)F\frac{\partial^2 F}{\partial y^2}-\left(\frac{\partial F}{\partial y}\right)^2-\frac{\rho_f}{\rho_{nf}}\frac{\sigma_{nf}}{\sigma_f}M\frac{\partial F}{\partial y}+\left(\frac{\chi\rho_s\beta_s/\beta_f+(1-\chi)\rho_f}{\rho_{nf}}\right)\theta\frac{\sin x}{x}=x\left(\frac{\partial F}{\partial y}\frac{\partial^2 F}{\partial x\partial y}-\frac{\partial F}{\partial x}\frac{\partial^2 F}{\partial y^2}\right), \tag{15}$$

$$\frac{1}{\Pr}\left(\frac{k_{nf}/k_f}{(1-\chi)+\chi(\rho c_p)_s/(\rho c_p)_f}\right)\frac{\partial^2\theta}{\partial y^2}+F\frac{\partial\theta}{\partial y}(1+x\cot x)=x\left(\frac{\partial F}{\partial y}\frac{\partial\theta}{\partial x}-\frac{\partial F}{\partial x}\frac{\partial\theta}{\partial y}\right), \tag{16}$$

corresponding to the boundary conditions

$$F=\frac{\partial F}{\partial y}=0,\ \theta=1,\ \text{as}\ y=0,$$

$$\frac{\partial F}{\partial y}\to 0,\ \theta\to 0,\quad \text{as}\ y\to\infty, \tag{17}$$

At the lower stagnation point of the sphere$x\approx 0$, equations (15) and (16) can be reduced to the following ordinary differential equations:

$$\frac{\rho_f}{\rho_{nf}}\frac{1}{(1-\chi)^{2.5}}\left(1+\frac{1}{\beta}\right)F'''+2FF''-(F')^2-\frac{\rho_f}{\rho_{nf}}\frac{\sigma_{nf}}{\sigma_f}MF'+\left(\frac{\chi\rho_s\beta_s/\beta_f+(1-\chi)\rho_f}{(1-\chi)\rho_s+\chi\rho_f},\right)\theta=0, \tag{18}$$

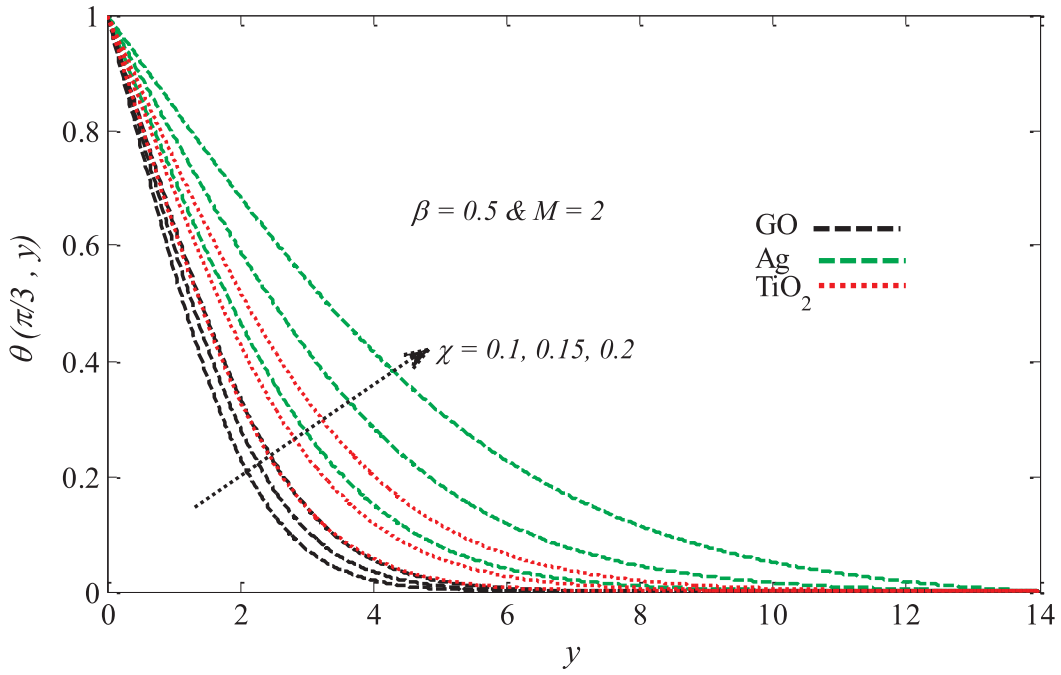

Fig. 9. χ vs $\theta(\pi/3, y)$

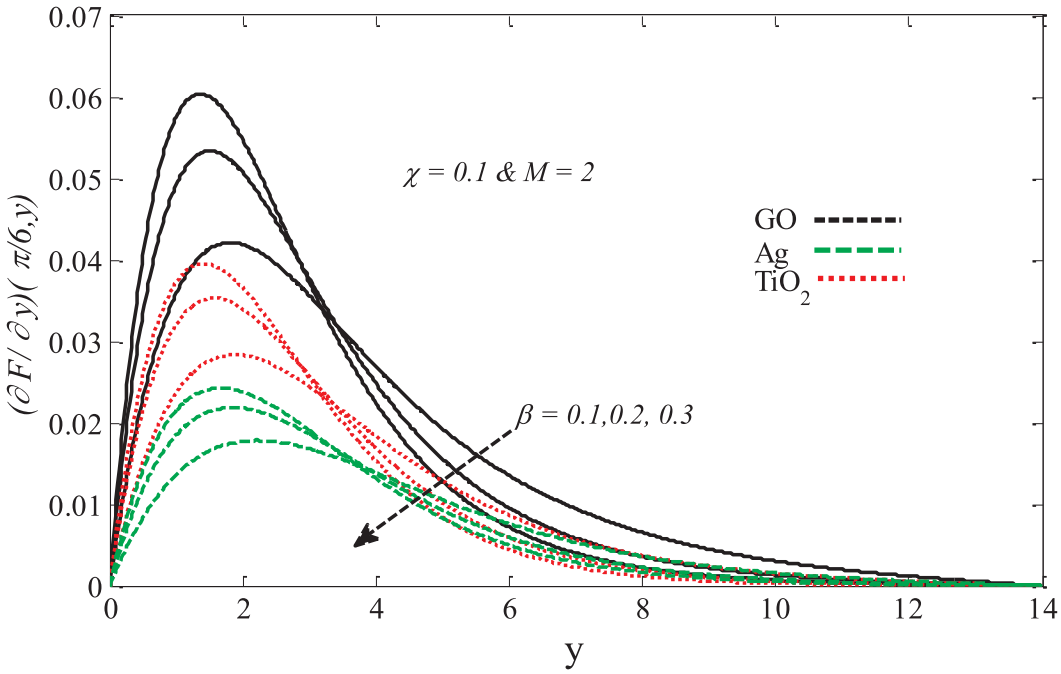

Fig. 10. β vs $(\partial F/\partial y)(\pi/6, y)$

$$\frac{1}{\Pr}\left(\frac{k_{nf}/k_f}{(1-\chi)+\chi(\rho c_p)_s/(\rho c_p)_f}\right)\theta'' + F\theta' = 0, \tag{19}$$

and the boundary conditions (17) can be written as follows:

$$F(0) = F'(0) = 0, \quad \theta(0) = 1 \quad \text{as } y = 0,$$

$$F' \to 0, \quad \theta \to 0 \quad \text{as } y \to \infty, \tag{20}$$

In this paper we focus on two physical quantities namely the local skin friction coefficient C_f and the local Nusselt number Nu, which are given by Molla et al. [34]:

$$C_f = \left(\frac{\tau_w}{\rho U_\infty^2}\right), \; Nu = \left(\frac{a q_w}{k_f(T_w - T_\infty)}\right), \tag{21}$$

where

$$\tau_w = \mu_{nf}\left(\frac{\partial u^*}{\partial y^*}\right)_{y^*=0}, \; q_w = -k_{nf}\left(\frac{\partial T}{\partial y^*}\right)_{y^*=0}. \tag{22}$$

By using (7) and (11), the local skin friction coefficient C_f and the local Nusselt numberNu become:

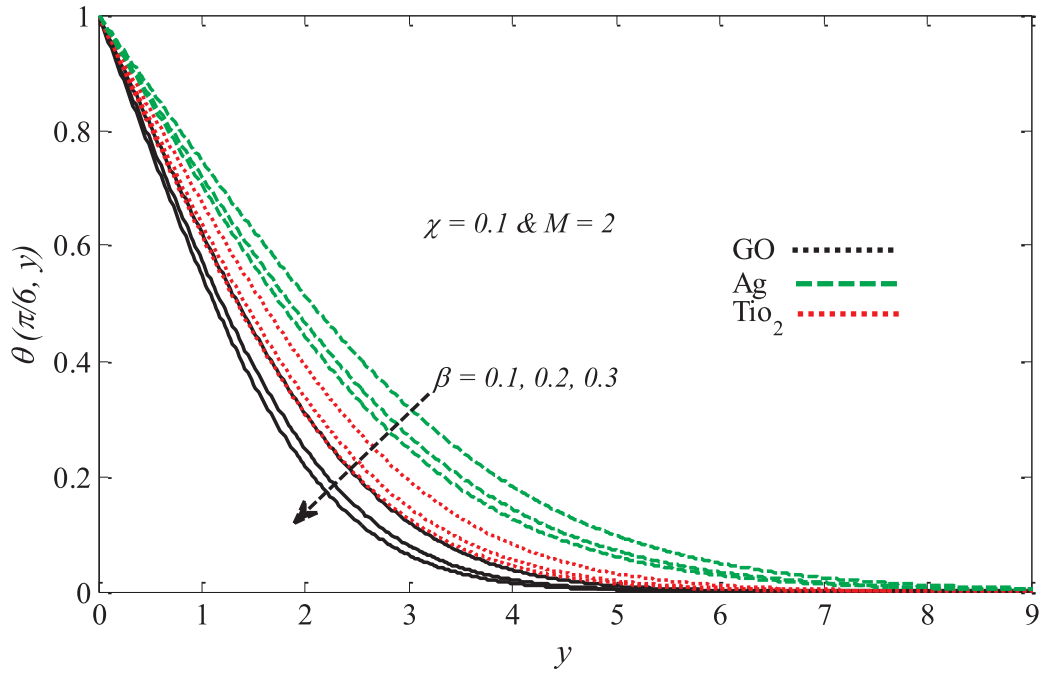

Fig. 11. β vs $\theta(\pi/6, y)$

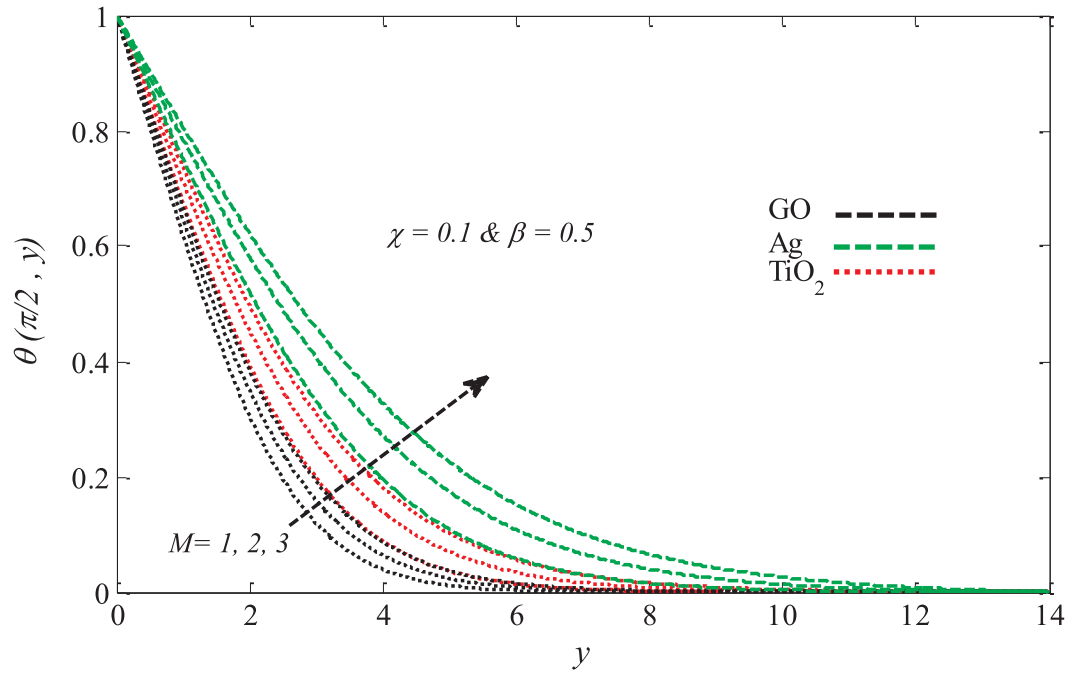

Fig. 12. Mvs $\theta(\pi/2, y)$

$$Gr^{1/4}C_f = \frac{1}{(1-\chi)^{2.5}}\left(1+\frac{1}{\beta}\right)x\frac{\partial^2 F}{\partial y^2}(x,0),$$
$$Gr^{-1/4}Nu = -\frac{k_{nf}}{k_f}\frac{\partial\theta}{\partial y}(x,0), \tag{23}$$

Numerical method

The nonlinear differential Eqs. (15) and (16) along with boundary conditions (17) are solved utilizing the Keller-box method. It is unconditionally stable with a second order convergence, simple for coding and the results are achieved in a reasonable time, the Keller-box method is depicted in Cebeci and Bradshaw [41], Hymavathi and Sridhar [42] and Malik et al. [43],where Eqs. (15) and (16) are initially reduced to first-order equations, then the difference equations are written using a central differences method, after that the obtained algebraic equations are linearized by Newton's method and finally the linear system is written in the matrix vector form and solved it by applying the block tridiagonal elimination technique. Here the boundary layer thickness $y_\infty = 18$ and the step size $\Delta y = 0.02$, $\Delta x = 0.005$ are adequate to give precise numerical results.

Results and discussions

In the present section, we have discussed the local skin friction

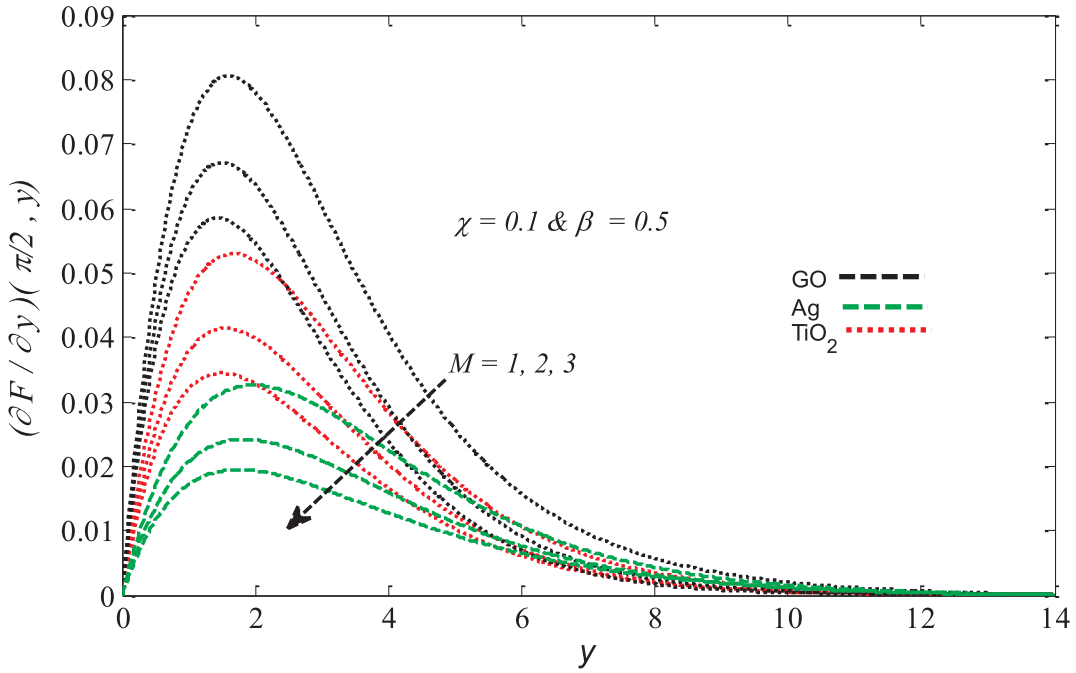

Fig. 13. M vs $(\partial F/\partial y)(\pi/2, y)$

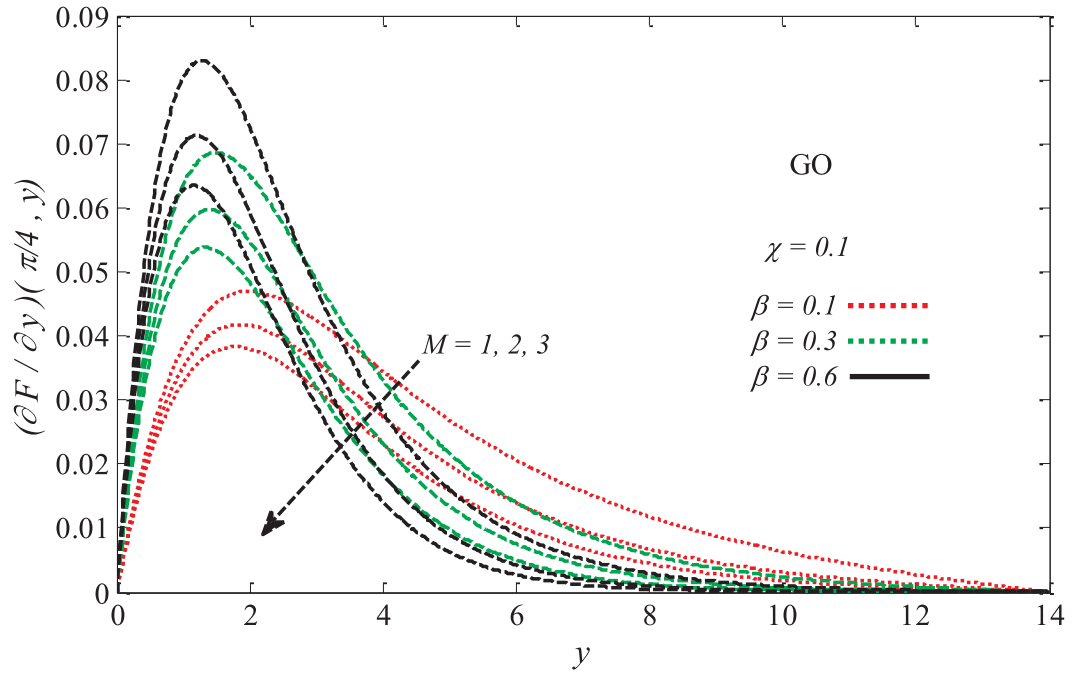

Fig. 14. (M and β) vs $(\partial F/\partial y)(\pi/4, y)$

coefficient $Gr^{1\backslash 4}C_f$, the local Nusselt number $Gr^{-1/4}Nu$, velocity profile $F'$and temperature profile θ for various physical parameters such as nanoparticle volume fraction χ, Casson fluid parameter β and magnetic parameter M, three types of nanoparticles Silver (Ag), Titanium dioxide (TiO_2) and Graphite oxide (GO) based on Sodium Alginate (SA) which is taken as a Casson host fluid. The magnetic parameter$M$ is varied from 1 to 3, the Casson parameter β is ranged from 0.1 to 0.5 and the values of nanoparticle volume fraction parameter χconsidered are 0.1, 0.15 and 0.2. The numerical results of nonlinear partial differential equations start at the lower stagnation point of the sphere $x \approx 0$, with initial profiles as given by the equation (19) to (21), and proceed round the sphere up to $x = 120^o$. Table 1 presents the thermo-physical properties of nanoparticles and based Casson fluid, Tables 2 displays the compatibility between the current result with preceding published results, we found that current results are in good agreement with the prior results published by Huang and Chen [44], Molla et al. [45] and Cheng [46].

Figs. 2–5 present the effect of nanoparticle volume fraction χ and Casson fluid parameter β on the local skin friction coefficient $Gr^{1/4}C_f$ and on the local Nusselt number Nu with various values of x for three types of nanoparticles Silver (Ag), Titanium dioxide (TiO_2) and Graphite oxide (GO) based on Sodium Alginate (SA). From these figures it is found that (GO)/(SA) based Casson nanofluid is higher than other nanoparticles/(SA) based Casson nanofluid. This is because the thermal

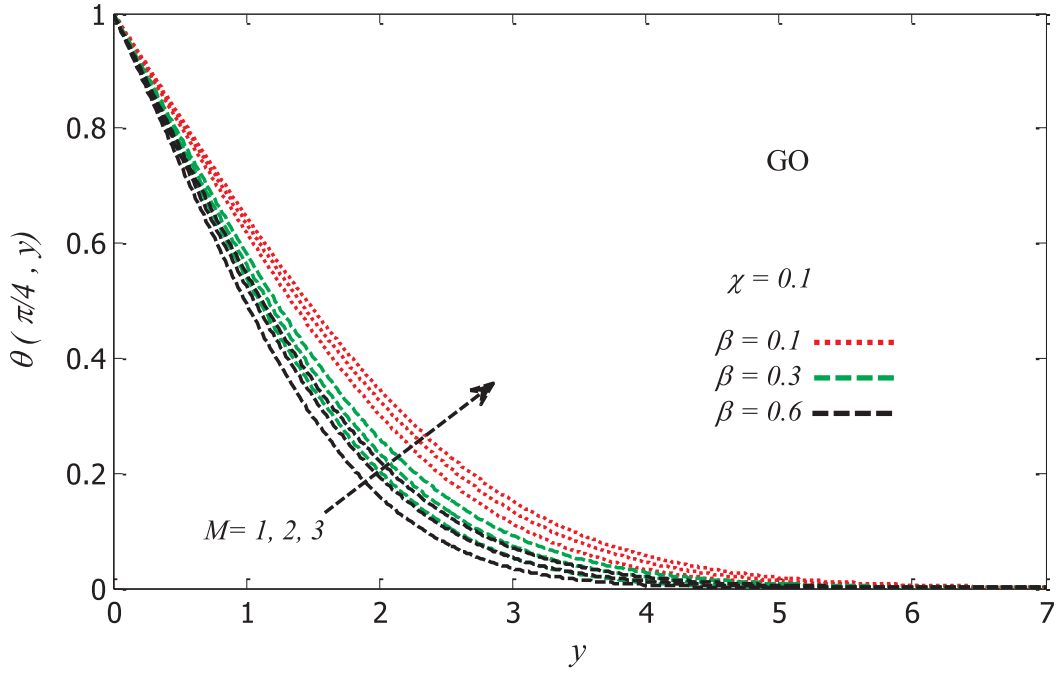

Fig. 15. (M and β) vs $\theta(\pi/4, y)$

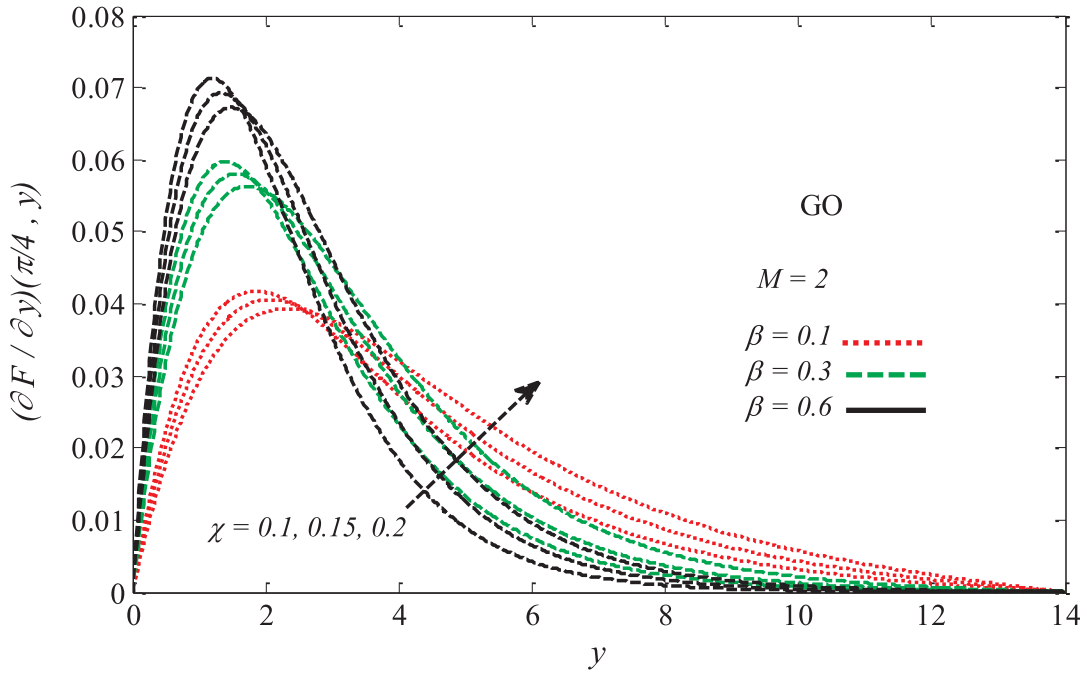

Fig. 16. (χ and β) vs $(\partial F/\partial y)(\pi/4, y)$

conductivity of GO is higher than the other nanoparticles hence this makes it more stable. Furthermore, the values of local skin friction coefficient $Gr^{1/4}C_f$ and the local Nusselt number $Gr^{-1\backslash 4}Nu$increase with increases of nanoparticle volume fraction χ, and as the Casson fluid parameter βincreases, the values of local skin friction coefficient $Gr^{1/4}C_f$ reduce but the local Nusselt number $Gr^{-1\backslash 4}Nu$increases.

The effect of magnetic parameter M on the local skin friction and local Nusselt number is shown in Figs. 6 and 7. It is seen that when the magnetic parameter M decreases, both local skin friction and local Nusselt number increases. The Intensity of magnetic field inside the boundary layer literally leads to increase the Lorentz force which significantly impacts the flow in the reverse direction. Consequently, it reduces the rates of local skin friction coefficient and local Nusselt number. It notes that the effect of nanoparticles components is itself as for previous figures, this is because the physical properties do not vary according to parameters.

Figs. 8 and 9 show the effect of nanoparticle volume fraction χ on velocity profiles and temperature profiles for three types of nanoparticles Graphite oxide (GO), Silver (Ag) and Titanium dioxide (TiO2) based on Sodium Alginate (SA). It can be seen the Graphite oxide (GO) has high velocity profiles compared to that other nanoparticles Sodium Alginate based Casson nanofluid, while the temperature profiles for Silver (Ag) are greater than the other nanoparticles Sodium Alginate based Casson nanofluid when nanoparticle volume fraction χ increases.

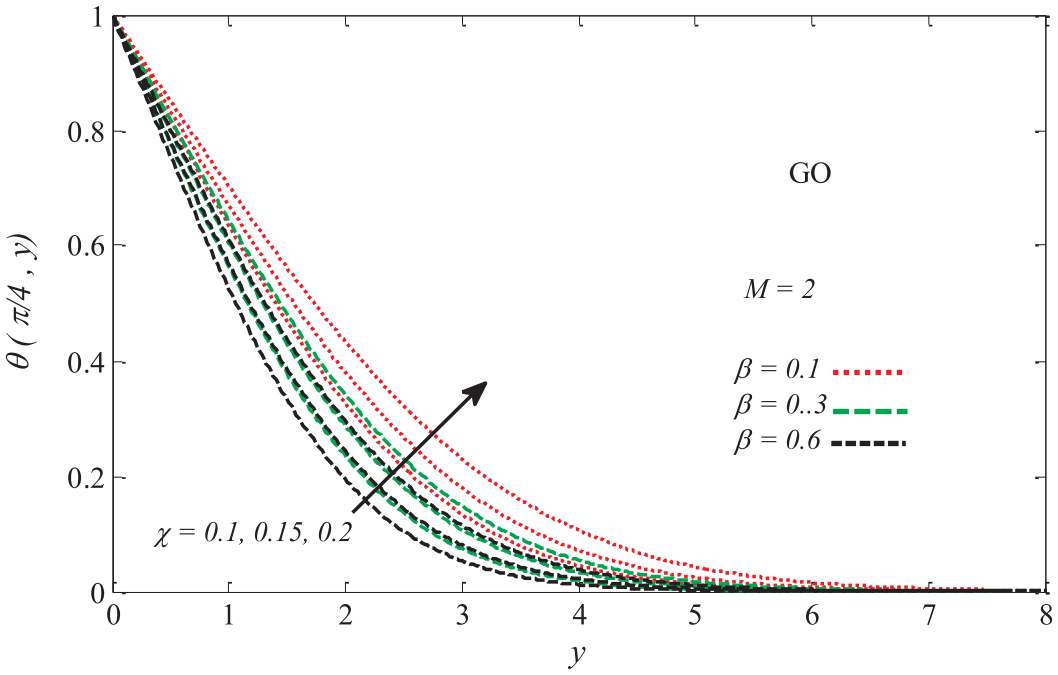

Fig. 17. (χ and β) vs $\theta\,\pi/4,\ y$)

Figs. 10 and 11 also show the velocity profiles and temperature profiles comparison of three types of nanoparticles Graphite oxide (GO), Silver (Ag) and Titanium dioxide (TiO2) based on Sodium Alginate (SA) with variouse values of Casson fluid parameter β It is observed that also Graphite oxide (GO) has high velocity profiles, but the temperature is higher for Silver (Ag) based Casson nanofluid than for Graphite oxide (GO) and Titanium dioxide (TiO_2) based on Sodium Alginate (SA) with decrease in Casson fluid parameter

Figs. 12 and 13 show the impacts of various values of magnetic parameter M on temperature and velocity profiles with the same of types of nanoparticles in Figs. 2–11. The acquired numerical results illustrate that an increase magnetic parameter M led to increase the values of temperature profiles , but the values of the velocity decrease. This is compatible with the physical problems, since the transverse magnetic field produce a resistive force type (Lorentz force) such drag force which led to resist the fluid flow hence reducing its velocity.

Figs. 14 and 15 illustrate the impact of magnetic parameter M and Casson parameter β on the velocity and temperature profiles. It is observed that a decrease in β or M led to an increase in velocity and an increase in M or a decrease in β led to an increase in temperature.

Finally, in Figs. 16 and 17 the velocity and temperature profiles are evaluated at different values of χ and β. It can be noted that by increasing χ or decreasing β, the velocity profile increases and by increasing χ or reducingβ, the temperature profile increases.

Conclusions

In this work, steady laminar 2-D incompressible MHD natural convection flow of three different types of nanoparticles suspended Casson nanofluid on a solid sphere has been studied, the problem is solved by the Keller box method and the following conclusions are found:

i. Graphite oxide (GO) has high local skin friction, local Nusselt number and velocity profile compared to other nanoparticles Sodium Alginate based Casson nanofluid.
ii. Temperature of Silver (Ag) based Casson nanofluid is higher than other nanoparticles based Casson nanofluid with decreases of Casson parameterβ and increases of magnetic parameter M.
iii. When the nanoparticle volume fraction χ increases, the local skin friction, local Nusselt number, velocity and temperature profiles increase.
iv. When Casson parameter β increases, the local skin friction coefficient and the local Nusselt number increase, but temperature and velocity profiles decrease
v. When the magnetic parameter M increases, the local Nusselt number $Gr^{-1/4}Nu$, local skin friction coefficient $Gr^{1\backslash 4}C_f$, velocity profiles decrease, while the temperature profiles increase.

Acknowledgment

The authors would like to acknowledge University Malaysia Terengganu (UMT) for the financial support through grant vote numbers 55193/4 for this research.

References

[1] Stanford E. Manufacture of useful products from seaweeds. Great Britain; 1881.
[2] Stanford E. ON algin, a new substance obtained from some of the commoner species of marine Algae. Am J Pharm 1883;47:617.
[3] Hatami M, Ganji D. Heat transfer and flow analysis for SA-TiO2 non-Newtonian nanofluid passing through the porous media between two coaxial cylinders. J Mol Liq 2013;188:155–61.
[4] Hatami M, Ganji D. Natural convection of sodium alginate (SA) non-Newtonian nanofluid flow between two vertical flat plates by analytical and numerical methods. Case Stud Therm Eng 2014;2:14–22.
[5] Akinshilo AT, Olofinkua JO, Olaye O. Flow and heat transfer analysis of the sodium alginate conveying copper nanoparticles between two parallel plates. J Appl Computat Mechan 2017;3:258–66.
[6] Sharma B, Kumar S, Paswan M. Numerical investigation of MHD stagnation-point flow and heat transfer of sodium alginate non-Newtonian nanofluid. Nonlin Eng 2018.
[7] Ahmed TN, Khan I. Mixed convection flow of sodium alginate (SA-NaAlg) based molybdenum disulphide (MoS2) nanofluids: Maxwell Garnetts and Brinkman models. Results Phys 2018;8:752–7.
[8] Tlili I, Khan W, Khan I. Multiple slips effects on MHD SA-Al2O3 and SA-Cu non-Newtonian nanofluids flow over a stretching cylinder in porous medium with radiation and chemical reaction. Results Phys 2018;8:213–22.
[9] Chol S, Estman J. Enhancing thermal conductivity of fluids with nanoparticles. ASME-Publications-Fed 1995;231:99–106.
[10] Buongiorno J. Convective transport in nanofluids. J Heat Transfer 2006;128:240–50.
[11] Tiwari RK, Das MK. Heat transfer augmentation in a two-sided lid-driven differentially heated square cavity utilizing nanofluids. Int J Heat Mass Transf 2007;50:2002–18.
[12] Sheremet MA, Grosan T, Pop I. Free convection in a square cavity filled with a

porous medium saturated by nanofluid using Tiwari and Das' nanofluid model. Transp Porous Media 2015;106:595–610.
[13] Sheremet MA, Pop I, Bachok N. Effect of thermal dispersion on transient natural convection in a wavy-walled porous cavity filled with a nanofluid: Tiwari and Das' nanofluid model. Int J Heat Mass Transf 2016;92:1053–60.
[14] Sheremet MA, Pop I, Shenoy A. Natural convection in a wavy open porous cavity filled with a nanofluid: Tiwari and Das' nanofluid model. Eur Phys J Plus 2016;131:62.
[15] Sheremet MA, Dinarvand S, Pop I. Effect of thermal stratification on free convection in a square porous cavity filled with a nanofluid using Tiwari and Das' nanofluid model. Physica E 2015;69:332–41.
[16] Ghalambaz M, Sheremet MA, Pop I. Free convection in a parallelogrammic porous cavity filled with a nanofluid using Tiwari and Das' nanofluid model. PLoS ONE 2015;10. e0126486.
[17] Matin MH, Pop I. Forced convection heat and mass transfer flow of a nanofluid through a porous channel with a first order chemical reaction on the wall. Int Commun Heat Mass Transfer 2013;46:134–41.
[18] Sheikholeslami M. Numerical investigation for CuO-H2O nanofluid flow in a porous channel with magnetic field using mesoscopic method. J Mol Liq 2018;249:739–46.
[19] Hussanan A, Khan I, Gorji MR, Khan WA. CNT S-Water–Based Nanofluid Over a Stretching Sheet. BioNanoScience 2019;9:21–9.
[20] Nield D, Kuznetsov A. The Cheng-Minkowycz problem for natural convective boundary-layer flow in a porous medium saturated by a nanofluid. Int J Heat Mass Transf 2009;52:5792–5.
[21] Kuznetsov A, Nield D. Natural convective boundary-layer flow of a nanofluid past a vertical plate. Int J Therm Sci 2010;49:243–7.
[22] Kuznetsov A, Nield D. The Cheng-Minkowycz problem for natural convective boundary layer flow in a porous medium saturated by a nanofluid: a revised model. Int J Heat Mass Transf 2013;65:682–5.
[23] Kuznetsov A, Nield D. Natural convective boundary-layer flow of a nanofluid past a vertical plate: a revised model. Int J Therm Sci 2014;77:126–9.
[24] Sheikholeslami M, Gorji-Bandpy M, Ganji D. Numerical investigation of MHD effects on Al2O3–water nanofluid flow and heat transfer in a semi-annulus enclosure using LBM. Energy 2013;60:501–10.
[25] Das S K, Choi S U, Yu W,Pradeep T. John Wiley & Sons; 2007.
[26] Hussanan A, Salleh MZ, Alkasasbeh HT, Khan I. MHD flow and heat transfer in a casson fluid over a nonlinearly stretching sheet with newtonian heating. Heat Transf Res 2018;49.
[27] Trisaksri V, Wongwises S. Critical review of heat transfer characteristics of nanofluids. Renew Sust Energy Rev 2007;11:512–23.
[28] Wang X-Q, Mujumdar AS. A review on nanofluids-part I: theoretical and numerical investigations. Braz J Chem Eng 2008;25:613–30.
[29] Kumari M, Takhar H, Nath G. Compressible MHD boundary layer in the stagnation region of a sphere. Int J Eng Sci 1990;28:357–66.
[30] Nazar R, Amin N. Free convection boundary layer on an isothermal sphere in a micropolar fluid. Int Commun Heat Mass Transfer 2002;29:377–86.
[31] Chamkha AJ, Al-Mudhaf A. Simultaneous heat and mass transfer from a permeable sphere at uniform heat and mass fluxes with magnetic field and radiation effects. Numer Heat Transfer Part A 2004;46:181–98.
[32] Alkasasbeh HT. Numerical solution of micropolar casson fluid behaviour on steady MHD natural convective flow about a solid sphere. J Adv Res Fluid Mechan Therm Sci 2018;50:55–66.
[33] Molla MM, Taher M, Chowdhury MM, Hossain MA. Magnetohydrodynamic natural convection flow on a sphere in presence of heat generation. Nonlin Anal: Modell Control 2005;10:349–63.
[34] Molla M, Hossain M, Taher M. Magnetohydrodynamic natural convection flow on a sphere with uniform heat flux in presence of heat generation. Acta Mech 2006;186:75.
[35] Bég OA, Zueco J, Bhargava R, Takhar HS. Magnetohydrodynamic convection flow from a sphere to a non-Darcian porous medium with heat generation or absorption effects: network simulation. Int J Therm Sci 2009;48:913–21.
[36] Haque MR, Alam MM, Ali M, Sheikh MN. Effects of viscous dissipation on MHD natural convection flow over a sphere with temperature dependent thermal conductivity in presence of heat generation. ESJ 2014;10.
[37] Zangooee M, Hosseinzadeh K, Ganji D. Hydrothermal analysis of MHD nanofluid (TiO2-GO) flow between two radiative stretchable rotating disks using AGM. Case Stud Therm Eng 2019;14. 100460.
[38] Tabassum R, Mehmood R, Akbar N. Magnetite micropolar nanofluid non-aligned MHD flow with mixed convection. Eur Phys J Plus 2017;132:275.
[39] Takabi B, Shokouhmand H. Effects of Al 2 O 3–Cu/water hybrid nanofluid on heat transfer and flow characteristics in turbulent regime. Int J Mod Phys C 2015;26:1550047.
[40] Swalmeh MZ, Alkasasbeh HT, Hussanan A, Mamat M. Heat transfer flow of Cu-water and Al2O3-water micropolar nanofluids about a solid sphere in the presence of natural convection using Keller-box method. Results Phys 2018;9:717–24.
[41] Cebeci T, Bradshaw P. New York:Springer Science & Business Media; 2012.
[42] Hymavathi T, Sridhar W. Numerical solution to Diffusion of Chemically Reactive Species of a Casson Fluid Flow over an Exponentially Stretching Surface.
[43] Malik M, Khan M, Salahuddin T, Khan I. Variable viscosity and MHD flow in Casson fluid with Cattaneo-Christov heat flux model: Using Keller box method. Eng Sci Technol Int J 2016;19:1985–92.
[44] Huang M,Chen C. Erratum: "Laminar Free Convection From a Sphere With Blowing and Suction"(Journal of Heat Transfer, 1987, 109, pp. 529–532). J Heat Transf 1991: 113: 548-548.
[45] Molla MM, Rahman A, Rahman LT. Natural convection flow from an isothermal sphere with temperature dependent thermal conductivity. J Naval Architect Mar Eng 2005;2:53–64.
[46] Cheng C-Y. Natural convection heat and mass transfer from a sphere in micropolar fluids with constant wall temperature and concentration. Int Commun Heat Mass Transfer 2008;35:750–5.
[47] Hakeem AA, Saranya S, Ganga B. Comparative study on Newtonian/non-Newtonian base fluids with magnetic/non-magnetic nanoparticles over a flat plate with uniform heat flux. J Mol Liq 2017;230:445–52.
[48] Mahdy A. Simultaneous impacts of MHD and variable wall temperature on transient mixed Casson nanofluid flow in the stagnation point of rotating sphere. Appl Math Mech 2018;39:1327–40.
[49] Saranya S, Ragupathi P, Ganga B, Sharma R, Hakeem AA. Non-linear radiation effects on magnetic/non-magnetic nanoparticles with different base fluids over a flat plate. Adv Powder Technol 2018;29:1977–90.